



## Capture and conversion of carbon dioxide by solar heat localization

Journal:	<i>Sustainable Energy &amp; Fuels</i>
Manuscript ID	SE-ART-11-2018-000546
Article Type:	Paper
Date Submitted by the Author:	08-Nov-2018
Complete List of Authors:	<p>Kashyap, Varun ; University of Houston System, Mechanical Engineering            Medhi, Riddhiman; University of Houston System, Department of Chemistry            Irajizad, Peyman; University of Houston System, Mechanical Engineering            Jafari, Parham; University of Houston, Mechanical Engineering            Nazari, Masoumeh; University of Houston            Masoudi, Ali; University of Houston System, Department of Mechanical Engineering            Marquez, Maria; University of Houston, Chemical and Biomolecular Engineering            Lee, T. Randall; University of Houston, Department of Chemistry            Ghasemi, Hadi; University of Houston System, Mechanical Engineering</p>



# Sustainable Energy & Fuels

## ARTICLE

### Capture and conversion of carbon dioxide by solar heat localization

Varun Kashyap<sup>a</sup>, Riddhiman Medhi<sup>b</sup>, Peyman Irajizad<sup>a</sup>, Parham Jafari<sup>a</sup>, Masoumeh Nazari<sup>a</sup>, Ali Masoudi<sup>a</sup>, Maria D. Marquez<sup>b</sup>, T. Randall Lee<sup>b†</sup>, and Hadi Ghasemi<sup>a†</sup>

Received 00th January 20xx,  
Accepted 00th January 20xx

DOI: 10.1039/x0xx00000x

[www.rsc.org/](http://www.rsc.org/)

As the world slowly transitions from conventional fossil fuels to renewable forms of energy, environmentally friendly CO<sub>2</sub> capture is urgently needed. Currently, liquid amine and ionic liquid-based systems are utilized for this purpose. However, these forms of capture mostly lead to the formation of stable carbamate salts with high enthalpy of formation, and it is therefore difficult to recover the initial liquid for cyclic operation. Furthermore, amine-based technologies pose concerns including toxic emissions and volatility, while ionic liquid-based systems suffer from complexity of liquid handling and high operational cost. Herein, we report a solid-state sustainable CO<sub>2</sub> collector (SCC), which is activated by solar heat localization. This stable cyclic SCC is based on ionic liquids and graphene aerogel, which undergoes solid-liquid phase change to efficiently capture and convert CO<sub>2</sub>. The SCC captures 0.2 moles of CO<sub>2</sub> for every mole of ionic liquid and converts the absorbed CO<sub>2</sub> into useful byproducts, including water and calcium carbonate in each cycle. A system prototype of the SCC is developed and demonstrated. The SCC provides a new and promising paradigm to efficiently capture and convert CO<sub>2</sub> using abundant solar energy to address global emissions and consequent environmental challenges.

## Introduction

Global CO<sub>2</sub> emissions have increased at an alarming rate of approximately 40% over the last 10 to 15 years,<sup>1</sup> with the rate expected to double by 2050.<sup>2</sup> As a consequence, the reduction of environmental CO<sub>2</sub> has major implications on the global society<sup>3</sup>, and its capture is being viewed as one of the most prominent means of decarbonization. Demands for efficient CO<sub>2</sub> capture technologies are driving the exploration of different mechanisms.<sup>4</sup> Current commercial technologies employed for CO<sub>2</sub> capture include the use of amine-based solvents, mainly monoethanolamine (MEA), diethanolamine, and methyldiethanolamine.<sup>5–7</sup> However, these forms of capture lead to the formation of stable carbamate/carbonate salts<sup>8</sup>, making it difficult to recover the amine-based solvent for cyclic operation. Furthermore, the large enthalpy of CO<sub>2</sub> capture reaction corresponds to highly energy intensive and costly cyclic systems.<sup>9,10</sup> Amine-based systems suffer from low CO<sub>2</sub> capture capacity,<sup>10</sup> toxicity,<sup>11</sup> loss of reagent due to evaporation, and equipment corrosion.<sup>12</sup> To address these drawbacks, ionic liquids (ILs) are being considered as an alternative for CO<sub>2</sub> capture systems.

Ionic liquids, which are salts with melting points below 100 °C,<sup>10</sup> have gained attention in various fields due to their tunable molecular structures,<sup>13</sup> ILs enjoy unique properties such as low volatility, nonflammability, high thermal stability, and high CO<sub>2</sub> solubility.<sup>14,15</sup> The aforementioned properties have made ILs a

desirable alternative to conventional methods of CO<sub>2</sub> capture.<sup>16,17</sup> Various imidazolium anion-based ILs have been studied, mainly in the liquid state for CO<sub>2</sub> capture involving both physisorption and chemisorption.<sup>10</sup> In physisorption, the CO<sub>2</sub> molecules occupy the intermolecular spaces of the ILs without forming any chemical bonds. Molecular interactions (mainly van der Waals forces) between the CO<sub>2</sub> and IL molecules, primarily the anionic part, is the mechanism behind the capture.<sup>18</sup> In chemisorption, which is also studied by functionalized cations and anions,<sup>19,20</sup> chemical reactions take place between the imidazolium nitrogen and CO<sub>2</sub>, mainly leading to the formation of carbamate salts. Similar to most amine-based technologies, to reuse ILs after a chemical reaction, it is required to reverse the CO<sub>2</sub> absorption and carbamate formation steps, making the process energy intensive and costly. Furthermore, irrespective of the type of absorption, ILs are mainly used in the liquid state, which adds additional complexities including fluid lines, pumps, and other operational structures. As a result, research has been devoted to find methods for efficient and cyclic CO<sub>2</sub> capture in the form of solid-state material structures. In this study, a new solid-state approach and the related material paradigm called "sustainable CO<sub>2</sub> collector" (SCC), illustrated in Fig. 1, is proposed for CO<sub>2</sub> capture and conversion. This approach is cyclic, scalable, energy efficient, and non-toxic. The process also produces beneficial calcium carbonate, which is used in water treatment, manufacturing of cement, plaster, and mortars.<sup>21</sup> The SCC structure is comprised of ILs incorporated in a graphene aerogel matrix. To develop a stable material structure, the IL in

<sup>a</sup> Department of Mechanical Engineering, University of Houston, Houston, TX 77204-4006, USA

<sup>b</sup> Department of Chemistry and the Texas Center for Superconductivity, University of Houston, Houston, TX 77204-5003, USA

† Correspondence to [hghasemi@uh.edu](mailto:hghasemi@uh.edu) and [trlee@uh.edu](mailto:trlee@uh.edu)

Electronic Supplementary Information (ESI) available: [details of any supplementary information available should be included here]. See DOI: 10.1039/x0xx00000x

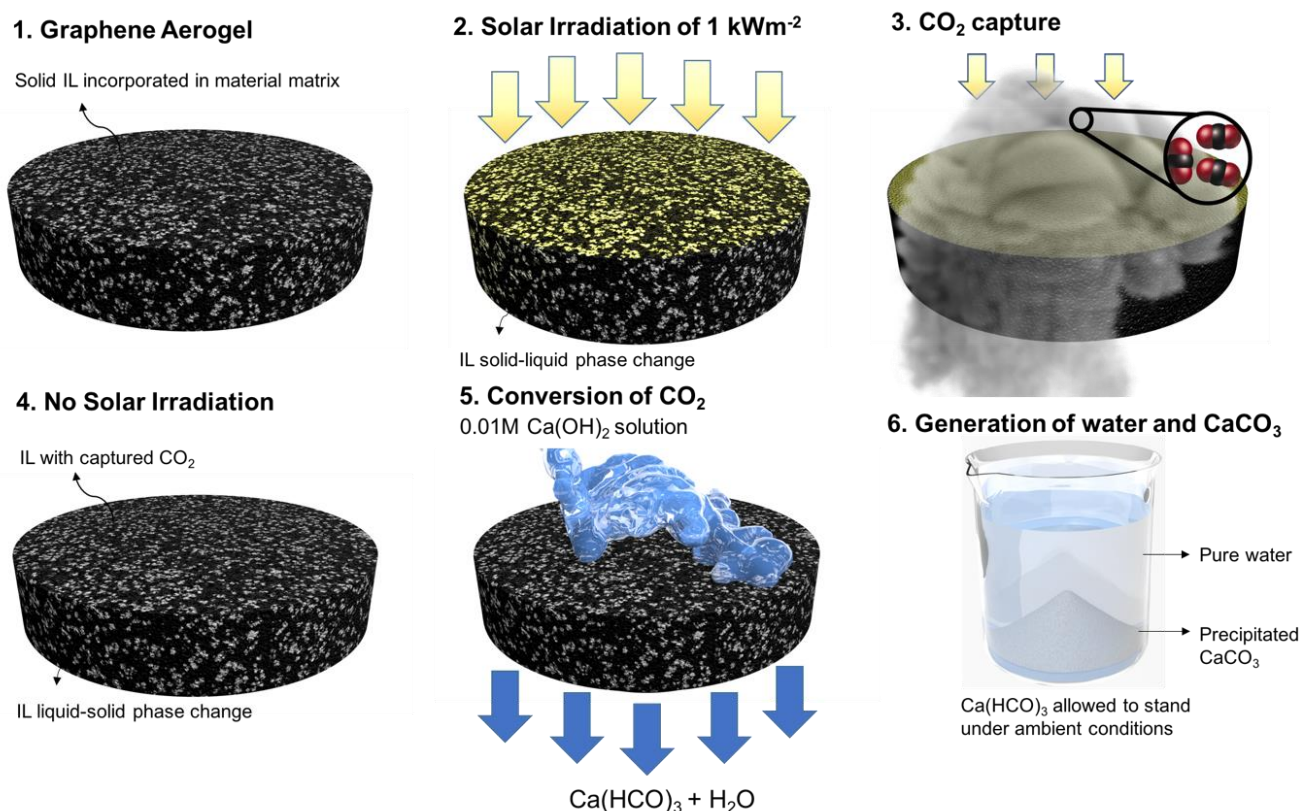


**Fig. 1.** Cyclic  $\text{CO}_2$  capture and its subsequent conversion to water and  $\text{CaCO}_3$ . Steps 1 and 2 illustrate the structure of the SCC and the solid-liquid phase change initiated by heat localization. Steps 3 and 4 show the capture of  $\text{CO}_2$  into the SCC. Steps 5 and 6 illustrate the washing and subsequent precipitation of  $\text{CaCO}_3$ . (A video on prototype of this cyclic SCC is shown in movie S1)

the SCC exists in the solid state. However,  $\text{CO}_2$  capture capacity for ILs in the liquid state is higher than that in the solid state. To stimulate solid-liquid phase change, we utilize the concept of solar heat localization. Neumann et al<sup>22</sup> and Ghasemi et al<sup>23</sup> introduced the concept of heat localization at the liquid-vapor interface for solar steam generation. Here, the material structure concentrates the thermal energy (provided by solar irradiation) needed for phase change while minimizing energy losses. Plasmonic nanoparticles and carbon-based material structures were studied to implement this concept.<sup>24–26</sup> For heat localization, the material matrix must possess the following properties: high volumetric absorption in the solar spectrum and low thermal conductivity to localize thermal energy. In addition to heat localization for solid-liquid phase change, the material should contain the ionic liquid for  $\text{CO}_2$  capture. Therefore, the material must possess high permeability to hold large volumes of the ionic liquid, hydrophobicity to avoid the retention of water in the material matrix, and oleophilicity to wet and retain the ionic liquid. Therefore, graphene aerogels were used for the SCC material matrix. Steps 1 and 2 in Fig. 1 show the IL integrated within the graphene aerogel. The process of integration is presented in the Supplementary Information. Due to heat localization, a temperature above the melting point of the IL is reached within the graphene aerogel, thereby facilitating solid-liquid phase change in the IL. In Step 3,  $\text{CO}_2$  gas is passed through the SCC for absorption. Once the SCC absorbs the  $\text{CO}_2$  and is no longer exposed to solar irradiation, the IL in the SCC goes back to its

solid state as shown in Step 4. In Step 5, the SCC is washed with dilute ( $0.01 \text{ M}$ )  $\text{Ca(OH)}_2$  solution. The absorbed  $\text{CO}_2$  in the IL reacts with this solution to form  $\text{Ca(HCO}_3)_2$  filtrate. The  $\text{Ca(HCO}_3)_2$  precipitates out as  $\text{CaCO}_3$  in Step 6, thereby leaving behind pure water. We emphasize that this cycle is repeatable, and the same SCC can be used to continuously capture  $\text{CO}_2$  and precipitate  $\text{CaCO}_3$  as the byproduct. A prototype has been developed to demonstrate the continuous operation of the SCC and is described in the Supplementary Information (Fig. S9). Note that the price of precipitated  $\text{CaCO}_3$  is  $\sim \$7/\text{kg}$  more than  $\text{Ca(OH)}_2$  and is also used in a wide range of industries.

## Results and Discussion

### Heat localization, effect of phase change, and selection of ILs<sup>[SEP]</sup>

Fig. 2 shows the effect of phase change on  $\text{CO}_2$  capture in the SCC. To initiate the solid-liquid phase change, graphene aerogel is used for heat localization. Graphene aerogel was synthesized to serve as the matrix material following a previously reported method;<sup>27</sup> synthetic details are provided in the Supplementary Information. An optical image of the graphene aerogel is shown in Fig. S1. To evaluate solar heat localization of the graphene aerogel, we measured its temperature as a function of time under solar irradiation of  $1 \text{ kWm}^{-2}$  and  $0.75 \text{ kWm}^{-2}$ . Furthermore, we compared its solar heat localization with other materials including exfoliated graphite and carbonized rayon. A

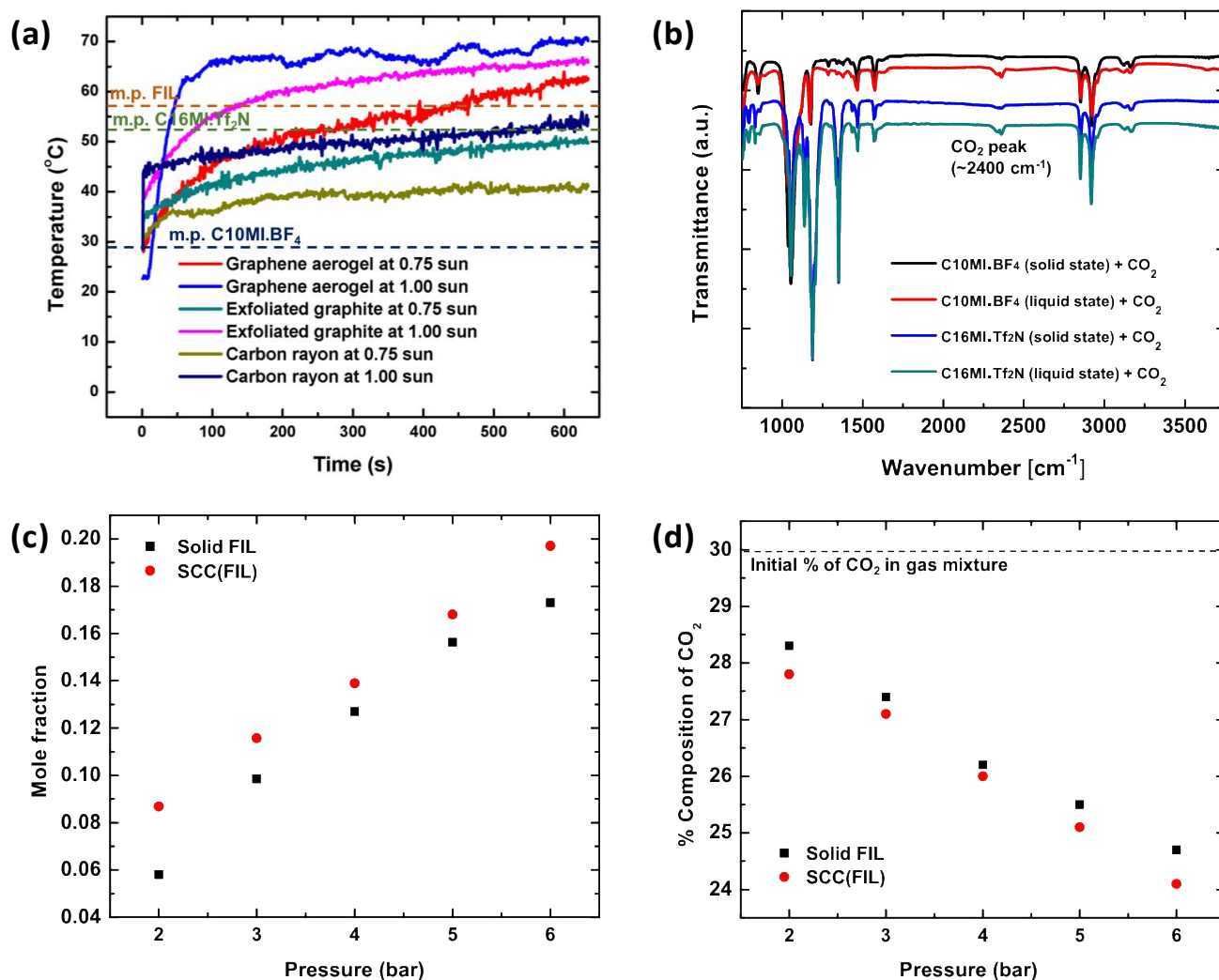


**Fig. 2.** The effect of phase change on CO<sub>2</sub> capture in ionic liquids is shown. (a) To initiate solid-liquid phase change, the concept of heat localization is used. Maximum temperature achieved by different materials at 1 sun and 0.75 sun solar illumination is shown. (b) FTIR measurements are conducted to evaluate capture of CO<sub>2</sub> in solid and liquid states, the average of two trials for each spectrum is reported here. (c) A plot of mole fraction of absorbed CO<sub>2</sub> as a function of pressure is shown. The SCC with the liquid-state ionic liquid shows higher capture compared to the SCC with the solid-state ionic liquid. (d) Percentage drop in CO<sub>2</sub> concentration is plotted as a function of pressure.

previously developed experimental setup was used to minimize side heat losses.<sup>28</sup> Fig. 2a shows the temperature increase as a function of time for these materials under 1 kWm<sup>-2</sup> and 0.75 kWm<sup>-2</sup> solar irradiation. As shown in the figure, the graphene aerogel at 1 sun solar irradiation reaches a higher temperature (~70°C) in comparison to exfoliated graphite and carbon rayon. This provides a wider melting point temperature range for the selection of ILs for the SCC. We therefore chose graphene aerogel as the material matrix to hold the ionic liquid in the SCC. The ILs chosen to be incorporated in graphene aerogel must have a melting point between 30 and 70 °C in order to show solid-liquid phase change under 1 kWm<sup>-2</sup> solar illumination and must contain imidazolium-based cations with high molecular weights and fluorinated anions for enhanced CO<sub>2</sub> absorption.<sup>18</sup> It is also desired to have ILs largely immiscible in water to avoid loss of ILs during the washing process with Ca(OH)<sub>2</sub> solution. Miscibility of ILs in water depends on the water-ion interaction strength, degree of fluorination, size of ions (larger fluorinated

ions are less miscible) and magnitude of the localized charge in the connecting atom.<sup>29</sup> Based on the above properties, two commercial ionic liquids were chosen, C10MI.BF<sub>4</sub> and C16MI.Tf<sub>2</sub>N. The structures of these ionic liquids are shown in Fig. S2. In addition to commercially available ionic liquids, we demonstrated CO<sub>2</sub> capture in ionic liquids with fluorinated cation groups. Fluorination of the cation can significantly improve the CO<sub>2</sub> solubility, although to a lesser extent than anion fluorination.<sup>30</sup> Fluorination of ionic liquids makes them more selective toward CO<sub>2</sub> absorption compared to alkyl chain cations.<sup>31</sup> Thus, to achieve enhanced CO<sub>2</sub> absorption in our system, we synthesized and utilized an imidazolium ionic liquid having more extensive fluorination than C10MI.BF<sub>4</sub> and C16MI.Tf<sub>2</sub>N, [CF<sub>3</sub>(CF<sub>2</sub>)<sub>7</sub>(CH<sub>2</sub>)<sub>3</sub>MI][(CF<sub>3</sub>CF<sub>2</sub>SO<sub>2</sub>)<sub>2</sub>N], henceforth abbreviated simply as fluorinated ionic liquid (FIL). The synthesis procedure is discussed in the Supplementary Information, and NMR confirmation of the product is provided in Fig. S3. This ionic liquid has a reported melting point of 56

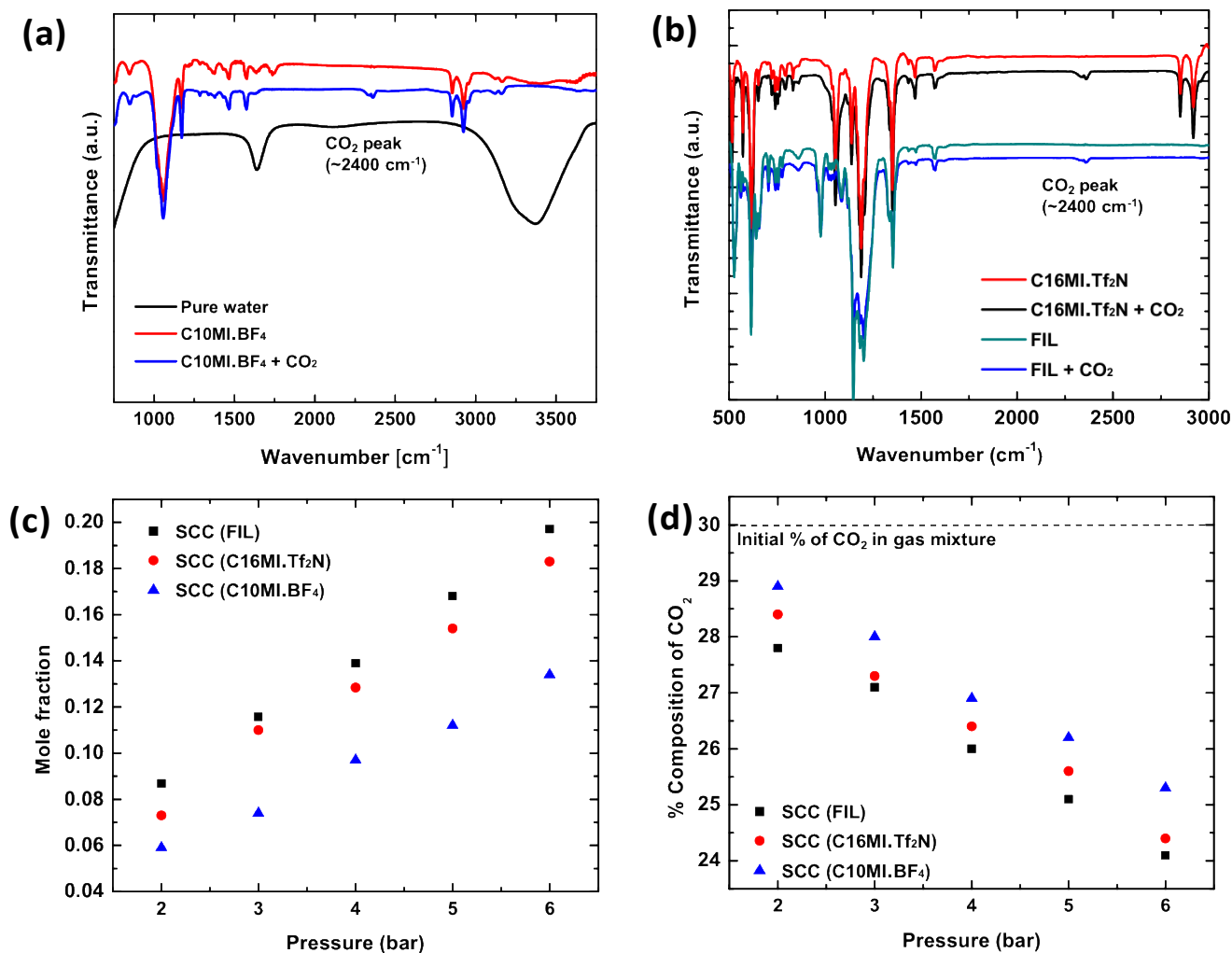


**Fig. 3.** CO<sub>2</sub> capture in the SCCs using various ionic liquids is shown. The effect of fluorination of the cation is demonstrated in these graphs. (a) FT-IR spectrum for the capture of CO<sub>2</sub> using C10MI.BF<sub>4</sub> ionic liquid. The presented FT-IR spectra are representative of 2 sets of measurements. Note that atmospheric CO<sub>2</sub> was purged out to ensure its absence from the spectra. (b) FT-IR spectrum for the CO<sub>2</sub> capture in C16MI.Tf<sub>2</sub>N and FIL are shown. (c) Pressure drop experiments were conducted using a high-pressure chamber to quantify the CO<sub>2</sub> capture in terms of mole fraction. (d) Change in percentage of CO<sub>2</sub> was quantified using a gas analyzer.

<sup>o</sup>C.<sup>32</sup> Note that SCC (X) is the general nomenclature used to represent a SCC composed from a specific IL - X, and so forth.

To study absorption of CO<sub>2</sub> in ILs in the solid and liquid states, we conducted three different experiments: FT-IR, mole fractions of captured CO<sub>2</sub>, and percentage change in CO<sub>2</sub> composition in the CO<sub>2</sub>-nitrogen mixture using the gas analyzer. Fig. 2b shows the FT-IR spectra for C10MI.BF<sub>4</sub> and C16MI.Tf<sub>2</sub>N ILs in the solid and liquid states. As shown, the intensity of the peak for CO<sub>2</sub> in the liquid sample is significantly higher than that in the solid state. Two separate experimental setups were developed, as described in the Supplementary Information (illustrated in Fig. S4 and Fig. S5) to quantify the amount of CO<sub>2</sub> captured by the SCC (FIL) with the FIL in the liquid state and in the solid state. In the first experiment, the pressure in the cylindrical high-pressure chamber was maintained between 2 bar and 6 bar for ~40 minutes. The mole fraction of CO<sub>2</sub> captured is shown in Fig. 2c. As shown, there is a difference of ~18-50% in CO<sub>2</sub> capture between FIL and SCC(FIL) depending on the CO<sub>2</sub> pressure, suggesting higher capture in the liquid state

than that in the solid state. In the second experiment, the change in the percentage composition of CO<sub>2</sub> was measured in the CO<sub>2</sub>-nitrogen mixture using the gas analyzer. Nitrogen is used in the gas mixture to demonstrate the selective absorption of the SCC toward CO<sub>2</sub>. As shown in Fig. 2d, the change in the CO<sub>2</sub> concentration is higher for SCC (FIL) in the liquid state, thereby indicating higher capture compared to FIL (solid state). Note that the percentage of nitrogen remains constant in the mixture. In Fig. 2d, we have studied a mixture of gases (N<sub>2</sub> and CO<sub>2</sub>), but in Fig. 2c, we have analyzed the SCC under pure CO<sub>2</sub>. Depending on the application, both scenarios might occur.

#### CO<sub>2</sub> capture using the sustainable CO<sub>2</sub> collector (SCCs)<sub>SEP</sub><sup>[17]</sup>

CO<sub>2</sub> absorption in the chosen ILs was quantified initially using a FT-IR method. Fig. 3a and Fig. 3b show the FT-IR spectra for ILs C10MI.BF<sub>4</sub>, C16MI.Tf<sub>2</sub>N, and FIL after CO<sub>2</sub> absorption, wherein a clear peak for CO<sub>2</sub> is seen at 2400 cm<sup>-1</sup>, in accordance with earlier reports of CO<sub>2</sub> FT-IR measurements.<sup>33</sup> To confirm that the peak is not due to atmospheric CO<sub>2</sub>, IR measurements were

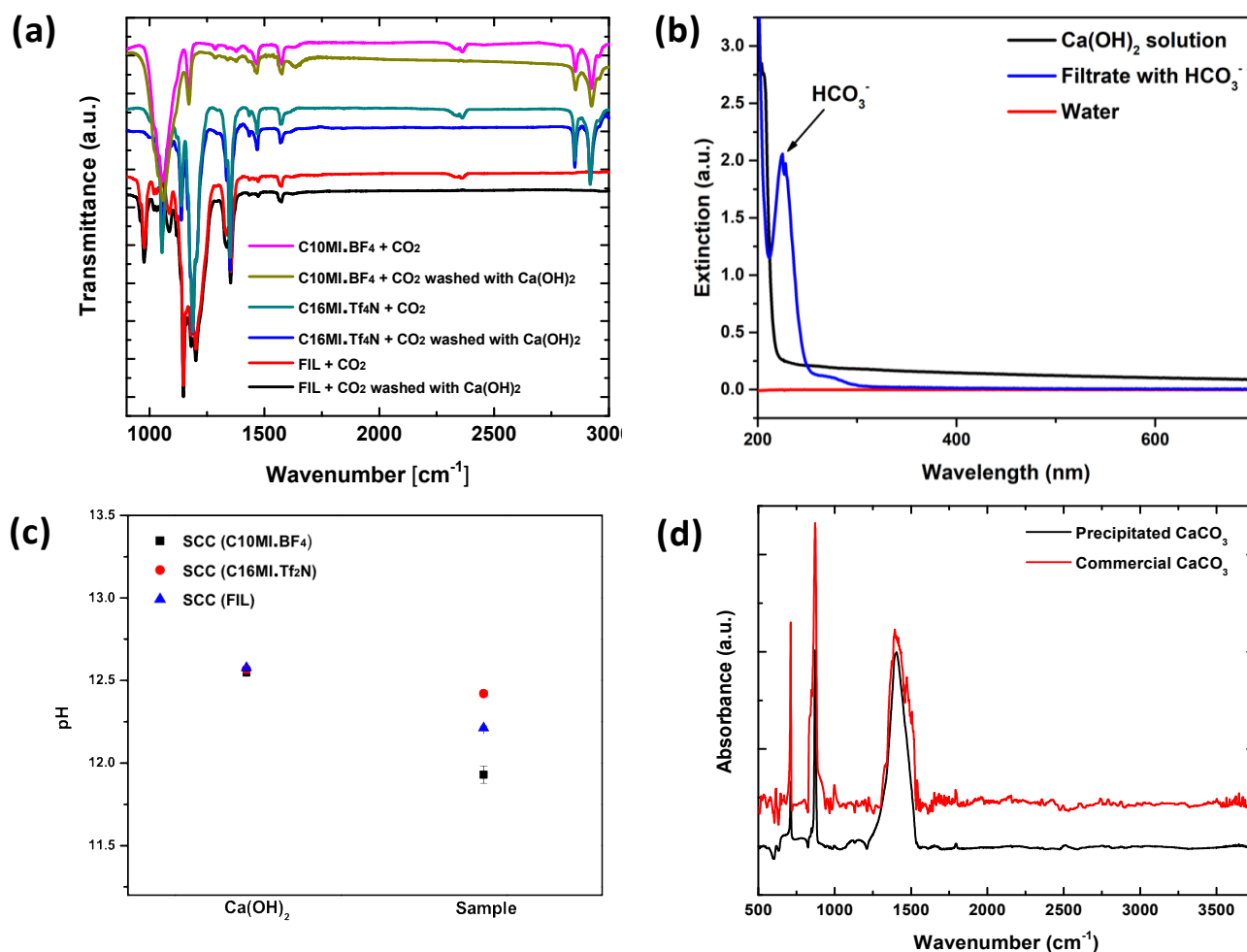


**Fig. 4.** Verification of the conversion of CO<sub>2</sub> to calcium bicarbonate and subsequently to CaCO<sub>3</sub>. (a) FT-IR spectrum to verify CO<sub>2</sub> present before and after washing with Ca(OH)<sub>2</sub> is shown. On washing with Ca(OH)<sub>2</sub>, the CO<sub>2</sub> peak at ~2400 cm<sup>-1</sup> disappears, thereby confirming the reaction of the absorbed CO<sub>2</sub> with the Ca(OH)<sub>2</sub>. (b) UV-vis spectrum is shown for the Ca(OH)<sub>2</sub> solution used for washing and for the filtrate formed after washing. The presence of Ca(HCO<sub>3</sub>)<sub>2</sub> in the filtrate is shown. Note that this UV-vis spectrum is taken as soon as the SCC is washed. (c) pH measurements were conducted to verify the formation of Ca(HCO<sub>3</sub>)<sub>2</sub> in the filtrate on washing with Ca(OH)<sub>2</sub>. A constant drop in pH can be seen in the filtrate. Note that these points are averaged over three trials. (d) FTIR spectrum for the final precipitated CaCO<sub>3</sub> is shown. This is in good agreement with the standard spectrum for CaCO<sub>3</sub>.

conducted after purging the compartment with nitrogen gas to remove atmospheric CO<sub>2</sub>. The IR spectrum of pure water was also obtained. Multiple trials consistently revealed a CO<sub>2</sub> peak for the IL samples only, verifying the capture of CO<sub>2</sub>. No changes were observed in the base IL patterns, thereby indicating that the CO<sub>2</sub> is absorbed in the ILs via physisorption. Furthermore, analysis of solid C16MI.Tf<sub>2</sub>N by <sup>13</sup>C NMR spectroscopy indicates CO<sub>2</sub> absorption as shown in Fig. S6 and Fig. S7.

Experimental setups similar to the ones described in the previous section (Fig. S4 and Fig. S5) were also used to quantify CO<sub>2</sub> capture in the SCC with the chosen ILs. Fig. 3c shows the mole fraction of CO<sub>2</sub> captured as a function of pressure. These experiments were conducted for the SCC (C16MI.Tf<sub>2</sub>N), SCC (C10MI.BF<sub>4</sub>), and SCC (FIL) samples. Solar irradiation of 1 sun was incident on the sample to stimulate solid-liquid phase change. The mole fraction of CO<sub>2</sub> captured is comparable to values reported in earlier literature for ILs.<sup>18</sup> As shown, the

capture in SCC (FIL) is slightly higher than SCC (C16MI.Tf<sub>2</sub>N) due probably to the higher degree of fluorination in the former IL. Fig. 3d shows the percentage drop of CO<sub>2</sub> as a function of pressure for SCC (C16MI.Tf<sub>2</sub>N), SCC (C10MI.BF<sub>4</sub>), and SCC (FIL). As shown in the figure, the maximum drop in percentage of CO<sub>2</sub> in the gas mixture is observed for SCC (FIL). This trend is consistent with the mole fraction of CO<sub>2</sub> captured for these ILs. The gas analyzer results confirm the absorption selectivity for CO<sub>2</sub> over N<sub>2</sub> as predicted based on previous studies.<sup>10</sup> Therefore, the selective capture of CO<sub>2</sub> in SCCs is confirmed from these experiments.

#### Conversion of the absorbed CO<sub>2</sub> to soluble HCO<sub>3</sub><sup>-</sup>

The chemical reactions involved in the reuse of the SCC for multiple cycles and conversion of the absorbed CO<sub>2</sub> to precipitated calcium carbonate are described in the Supplementary Information. The reaction of calcium hydroxide

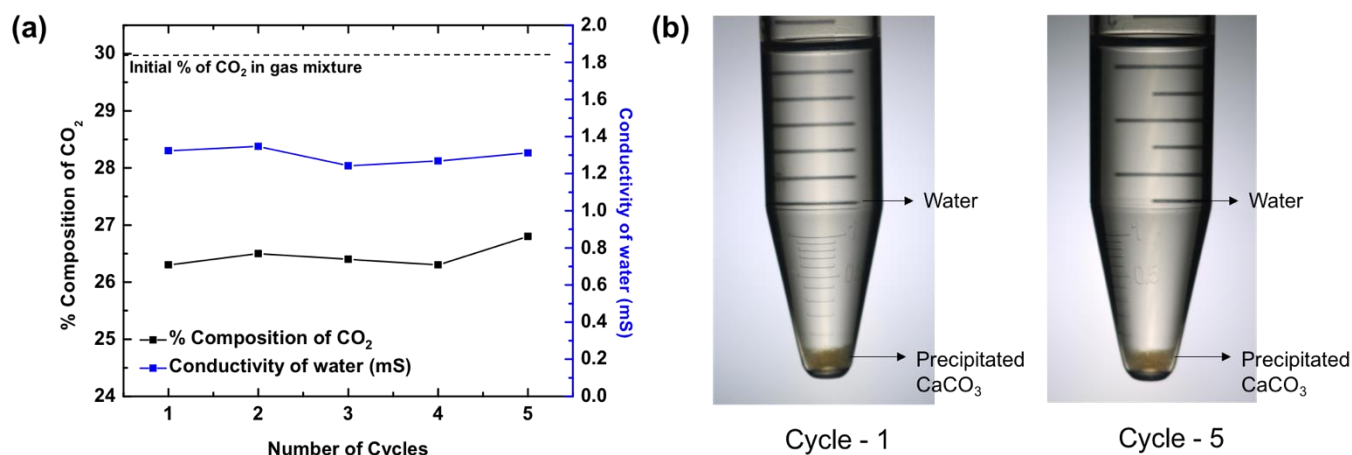


**Fig. 5.** The SCC is tested for repeatability over five cycles. (a) SCC (FIL) is used to capture  $\text{CO}_2$ , and the final percentage composition of  $\text{CO}_2$  is measured over five cycles. At  $\sim 4$  bar pressure, a nearly constant drop in the percentage of  $\text{CO}_2$  is observed in the gas mixture over multiple trials, thereby confirming the repeatability of the SCC. (b) Optical images of the byproducts including precipitated  $\text{CaCO}_3$  and water are shown for Cycle-1 and Cycle-5.

with  $\text{CO}_2$  to form calcium carbonate and calcium bicarbonate is well known.<sup>34</sup>  $\text{Ca}(\text{OH})_2$ , commonly called "slaked lime", primarily produces  $\text{CaCO}_3$  but forms  $\text{Ca}(\text{HCO}_3)_2$  in the presence of excess  $\text{CO}_2$ .<sup>35</sup> Both of these reactions are spontaneous.<sup>34</sup>

Solutions having low concentrations of  $\text{Ca}(\text{OH})_2$  in combination with an excess of  $\text{CO}_2$  selectively form the soluble  $\text{Ca}(\text{HCO}_3)_2$  species that is washed from the SCC. Fig. 4 shows the process of washing the SCC with  $\text{Ca}(\text{OH})_2$  to obtain precipitated  $\text{CaCO}_3$ . The absorption of  $\text{CO}_2$  into a  $\text{Ca}(\text{OH})_2$  solution is more efficient if the concentration of  $\text{Ca}(\text{OH})_2$  is low.<sup>10</sup> This is because lower concentrations of  $\text{Ca}(\text{OH})_2$  lead to  $\text{CO}_2$  absorbed in the solution, forming a mixture of mainly soluble bicarbonate ions.<sup>34</sup> We used a 0.01 M  $\text{Ca}(\text{OH})_2$  solution to wash the  $\text{CO}_2$  out of SCC (FIL). SCC (FIL), being mostly immiscible in water, remains unchanged, while the  $\text{CO}_2$  is converted to the soluble  $\text{HCO}_3^-$  species and is collected in the filtrate. Fig. 4a shows the FT-IR spectra for the disappearance of the  $\text{CO}_2$  peak at  $\sim 2400 \text{ cm}^{-1}$  after washing the ILs with this  $\text{Ca}(\text{OH})_2$  solution, confirming the effectiveness of the washing process.

Conversion of the  $\text{CO}_2$  to soluble  $\text{HCO}_3^-$  is confirmed by its presence in the filtrate via UV-Vis spectroscopy, as shown in Fig. 4b. Note that the UV-Vis spectrum was obtained soon after the SCC was washed with the  $\text{Ca}(\text{OH})_2$  solution. From these observations, the presence of  $\text{Ca}(\text{HCO}_3)_2$  in the filtrate can be confirmed, implying effective washing of the SCC and conversion of the absorbed  $\text{CO}_2$ . We then used an electronic pH meter (Mettler Toledo) with a measuring probe to compare the pH levels between the calcium hydroxide solution before and after washing the  $\text{CO}_2$ -impregnated SCCs. The experiment was conducted for the SCC containing all three different ionic liquids (C10MI.BF<sub>4</sub>, C16MI.Tf<sub>2</sub>N, and FIL) for three trials to confirm the reproducibility of the results. A drop in the pH was observed in the filtrate compared to the starting  $\text{Ca}(\text{OH})_2$  solution used for washing the ionic liquid, as shown in Fig. 4c. This experiment thus implicates the consumption of  $\text{OH}^-$  to form the less basic  $\text{HCO}_3^-$  species in solution, responsible for the drop in pH.<sup>36</sup>

#### Final conversion to precipitated $\text{CaCO}_3$ and reusability of the SCC

Soluble  $\text{HCO}_3^-$  is benign, but it is not the most commercially useful form of carbonate species. A conversion to a more useful product is desired. Precipitated  $\text{CaCO}_3$  enjoys widespread use in a variety of industries, including paints, plastics, papers, and sealants.<sup>21</sup> Therefore, to precipitate  $\text{CaCO}_3$  from  $\text{Ca}(\text{HCO}_3)_2$  solution, the solution was left to stand as reported by earlier studies.<sup>37</sup> Once the excess  $\text{CO}_2$  escapes from the solution, precipitated  $\text{CaCO}_3$  is left behind, which was verified by the FT-IR spectrum shown in Fig. 4d. The spectrum shows pure  $\text{CaCO}_3$  as compared to reference spectrum of commercial  $\text{CaCO}_3$ . Although in both cases of SCC(C16MI.Tf<sub>2</sub>N) and SCC(FIL), we recovered pure  $\text{CaCO}_3$ , in the case of SCC(C10MI.BF<sub>4</sub>), due to the low solubility of BF<sub>4</sub> anions in the water, we detected residual IL, as indicated by the C-H stretching peaks in the FT-IR spectrum in Fig. S10. Another method to precipitate calcium carbonate is to treat the bicarbonate filtrate with excess  $\text{Ca}(\text{OH})_2$  solution, which will precipitate out the calcium as calcium carbonate, as per Equation 3 in the Supplementary Information. Optical images for the products of this reaction are shown in Fig. S8. The final byproducts obtained from the SCC are  $\text{CaCO}_3$  and water. Note that the number of moles of  $\text{H}_2\text{O}$  formed is equal to the number of moles of  $\text{CO}_2$  absorbed.

To confirm the reusability of the SCCs, repeated  $\text{CO}_2$  absorption and washing over multiple cycles were conducted on SCC (FIL), since this proved to be the most efficient material based on the previous experiments. The gas analyzer set up and protocol (Fig. S5) was used to evaluate the reusability of the SCC. Fig. 5a shows the plot of percentage composition of  $\text{CO}_2$  in the resulting mixture as a function of repetition for 4 bar operating pressure. We found that the percentage composition of the final mixture remains constant even after 5 cycles, thereby demonstrating the excellent reusability of the SCCs. Fig. 5a shows the conductivity of water obtained from the reaction after the precipitation of  $\text{CaCO}_3$ . Similar conductivity is observed over five cycles as seen from the graph. Optical images of the byproducts including precipitated  $\text{CaCO}_3$  and water for the 1st and 5th cycles are shown in Fig. 5b. Furthermore, we should emphasize that the price of precipitated  $\text{CaCO}_3$  is  $\sim \$7/\text{kg}$  more than  $\text{Ca}(\text{OH})_2$ , which is the initial constituent of the reaction.

## Conclusions

In conclusion, we have developed a concept and corresponding material paradigm for reusable CO<sub>2</sub> capture while forming extremely useful precipitated CaCO<sub>3</sub>. Precipitated calcium carbonate has multiple applications including the manufacture of paints, plastics, papers, and sealants. Furthermore, the concept of heat localization with a graphene aerogel matrix was utilized to stimulate solid-liquid phase change, thereby increasing the CO<sub>2</sub> capture capacity. The use of solar energy further reduces the energy cost requirements for large scale implementation. We envision our SCC to be used for CO<sub>2</sub> capture during flue gas emission and the natural gas sweetening process. CO<sub>2</sub> capture in these applications will directly affect CO<sub>2</sub> concentration in the atmosphere. The next step for the implementation of this concept is to test the SCC in high pressure flue gas emission sites. We believe this concept and corresponding technology will assist in a smooth transition toward renewable energy sources.

## Acknowledgements

The authors gratefully acknowledge funding support from the Air Force Office of Scientific Research (Grant AFOSR FA9550-16-1-0248, H.G.) with Dr. Ali Sayir as program manager, Air Force Office of Scientific Research (Grant AFOSR FA9550-18-1-0094, T.R.L.), the Robert A. Welch Foundation (E-1320, T.R.L.) and the Texas Center for Superconductivity at the University of Houston (TcSUH, T.R.L.). They thank Dr. Jiming Bao of the University of Houston for help with FTIR measurements, Dr. Scott Smith for help with NMR measurements, and Abdullah Al-Bayati and Carlin Ashford for help with synthesis of graphene aerogels.

## References

- 1 IEA, CO<sub>2</sub> emissions from fuel combustion: Highlights. *Outlook*, 2010, **38**, 1–134.
- 2 International Energy Agency, *Energy Technology Perspectives: Scenarios & Strategies To 2050*, 2010.
- 3 IPCC, *Climate Change 2007 Synthesis Report*, 2007.
- 4 A. D. Ritter, J.A., Ebner, *separation science and technology*, 2009, **44**, 1273–1421
- 5 J. D. Figueroa, T. Fout, S. Plasynski, H. McIlvried and R. D. Srivastava, *Int. J. Greenh. Gas Control*, 2008, **2**, 9–20.
- 6 G. T. Rochelle, *Science*. (2009), **325**, 1652–1654..
- 7 B. Dutcher, M. Fan and A. G. Russell, *ACS Appl. Mater. Interfaces*, 2015, **7**, 2137–2148.
- 8 P. D. Vaidya and E. Y. Kenig, *Chem. Eng. Technol.*, 2007, **30**, 1467–1474.
- 9 O. F. Dawodu and A. Meisen, *Can. J. Chem. Eng.*, 1996, **74**, 960–966.
- 10 M. Ramdin, T. W. De Loos and T. J. H. Vlught, *Ind. Eng. Chem. Res.*, 2012, **51**, 8149–8177.
- 11 D. M. D'Alessandro, B. Smit and J. R. Long, *Angew. Chemie - Int. Ed.*, 2010, **49**, 6058–6082.
- 12 R. Davidson, *Clean Coal Cent*, 2007, **125**.
- 13 S. Zhang, N. Sun, X. He, X. Lu, and X. Zhang, *J. Phys. Chem*, 2006, **35**.
- 14 X. X. Zhang, X. X. Zhang, H. Dong, Z. Zhao, S. Zhang and Y. Huang, *Energy Environ. Sci.*, 2012, **5**, 6668.
- 15 J. F. Brennecke and B. E. Gurkan, *J. Phys. Chem. Lett.*, 2010, **1**, 3459–3464.
- 16 J. E. Bara, S. Lessmann, C. J. Gabriel, E. S. Hatakeyama, R. D. Noble and D. L. Gin, *Ind. Eng. Chem. Res.*, 2007, **46**, 5397–5404.
- 17 B. A. Voss, J. E. Bara, D. L. Gin and R. D. Noble, *Chem. Mater.*, 2009, **21**, 3027–3029.
- 18 C. Cadena, J. L. Anthony, J. K. Shah, T. I. Morrow, J. F. Brennecke and E. J. Maginn, *J. Am. Chem. Soc.*, 2004, **126**, 5300–5308.
- 19 E. D. Bates, R. D. Mayton, I. Ntai and J. H. Davis, *J. Am. Chem. Soc.*, 2002, **124**, 926–927.
- 20 B. E. Gurkan, J. C. de la Fuente, E. M. Mindrup, L. E. Ficke, B. F. Goodrich, E. A. Price, W. F. Schneider and J. F. Brennecke, *J. Am. Chem. Soc.*, 2010, **132**, 2116–2117.
- 21 O. A. Jimoh, K. S. Ariffin, H. Bin Hussin and A. E. Temitope, *Carbonates and Evaporites*, 2017, 1–16.
- 22 O. Neumann, A. S. Urban, J. Day, S. Lal, P. Nordlander and N. J. Halas, *ACS Nano*, 2013, **7**, 42–49.
- 23 H. Ghasemi, G. Ni, A. M. Marconnet, J. Loomis, S. Yerci, N. Miljkovic and G. Chen, *Nat. Commun.*, 2014, **5**, 4449.
- 24 G. W. Ni, S. H. Zandavi, S. M. Javid, S. V. Boriskina, T. A. Cooper and G. Chen, *Energy Environ. Sci.*, **1**, 2018, 1510–1519.
- 25 H. Song, Y. Liu, Z. Liu, M. H. Singer, C. Li, A. R. Cheney, D. Ji, L. Zhou, N. Zhang, X. Zeng, Z. Bei, Z. Yu, S. Jiang and Q. Gan, *Adv. Sci.*, 2018, 1800222.
- 26 J. Yang, Y. Pang, W. Huang, S. K. Shaw, J. Schifftbauer, M. A. Pillers, X. Mu, S. Luo, T. Zhang, Y. Huang, G. Li, S. Ptasinska, M. Lieberman and T. Luo, *ACS Nano*, 2017, **11**, 5510–5518.
- 27 L. M. Xu, G. Y. Xiao, C. B. Chen, R. Li, Y. Y. Mai, G. M. Sun and D. Y. Yan, *J. Mater. Chem. A*, 2015, **3**, 7498–7504.
- 28 V. Kashyap, A. Al-Bayati, S. M. Sajadi, P. Irajizad, S. H. Wang and H. Ghasemi, *J. Mater. Chem. A*, 2017, **5**, 15227–15234.
- 29 M. Klahn, C. Stüber, A. Seduraman and P. Wu, *J. Phys. Chem. B*, 2010, **114**, 2856–2868.
- 30 D. Almantariotis, T. Gefflaut, A. A. H. Pádua, J. Y. Coxam and M. F. Costa Gomes, *J. Phys. Chem. B*, 2010, **114**, 3608–3617.
- 31 D. Almantariotis, A. S. Pensado, H. Q. N. Gunaratne, C. Hardacre, A. A. H. Pádua, J.-Y. Coxam and M. F. Costa Gomes, *J. Phys. Chem. B*, 2017, **121**, 426–436
- 32 H. Ma, B. Chu and B. S. Hsiao, *Eur. Polym. J.*, 2017, **87**, 398–405.
- 33 S. U. Rege and R. T. Yang, *Chem. Eng. Sci.*, 2001, **56**, 3781–3796.
- 34 S.-J. Han, M. Yoo, D.-W. Kim and J.-H. Wee, *Energy & Fuels*, 2011, **25**, 3825–3834.
- 35 a M. Kalinkin, E. V. Kalinkina, O. a Zalkind and T. I. Makarova, *Inorg. Mater.*, 2005, **41**, 1073–1079.
- 36 Y. G. Bodlaender, *Angew. Chemie - Int. Ed*, **14**, 381–390 (1901).
- 37 Y. Kitano, *Bull. Chem. Soc. Jpn.*, 1962, **35**, 1973–1980.